Tunable surface patterning of azopolymer by vectorial holography: the role of photoanisotropies in the driving force

P. Pagliusi,[#,§,], B. Audia[#], C. Provenzano[#], M. Piñol[‡], L. Oriol[‡] and G. Cipparrone[#,§]*

[#] Dipartimento di Fisica, Università della Calabria, Ponte P. Bucci 31C, 87036 Rende (CS), Italy

[§] CNR-Nanotec and Centre of Excellence CEMIF.CAL, Ponte P. Bucci 33B, 87036 Rende (CS), Italy

[‡] Departamento de Química Orgánica, Instituto de Ciencia de Materiales de Aragón,Universidad de Zaragoza-CSIC, C/Pedro Cerbuna 12, 50009 Zaragoza, Spain

KEYWORDS

Surface relief gratings, azopolymer, polarization holography, reconfigurable topography, photoinduced birefringence

Abstract

The capability to pattern polymers surfaces at different length scales is an important goal in different research fields including display technologies, microelectronics, optics, as well as bio-related and medical science. However the ability to optically and dynamically manipulate topography is a key feature enabling remote control of associated effects/processes mediated by the surface. Azopolymers are largely investigated to this aim based on their sensitivity to optical fields and reconfigurability capabilities. In this work, surface relief formation induced by polarization patterns on an amorphous azopolymer structurally engineered to have large photoinduced birefringence, has been investigated both experimentally and theoretically. Based on the different light polarization patterns, depth and shape of the relief grating can be controlled. An optically induced gradient force model that includes both the spatial distribution and the anisotropy of the material permittivity has been theoretically analyzed. The proposed approach is able to explain the experimental results, and to overcome the limitation of existing models.

Introduction

Responsive polymers, i.e. polymers able to experience significant structural changes under external stimulation, have been largely investigated in the last twenty years.[1-5] Among them, azopolymers represent an interesting class of materials as the external stimulation is the light, which allows remote control in an easy and flexible way.[6] They have been widely investigated due to the large structural modification occurring under light irradiation. In such kind of polymers photoinduced isomerizations of the azobenzene units[7] can provide cooperative processes able to induce supramolecular orientation effects in the materials bulk and even matter motion bringing into topographical modifications.[8-17] Moreover, the reversibility of the involved photo-induced processes adds another interesting feature: the reconfigurability, i.e. the possibility to reinitialize it through additional thermal or optical treatment. With respect to the photo-induced effects, they are not only sensitive to the light intensity, but also to its polarization, increasing the control parameters able to affect optical and mechanical tasks addressed through them.[6, 12, 18, 19]

Based on these peculiarities, they were firstly investigated for reconfigurable optical storage and holographic interferometry applications in the optical and optoelectronics research areas.[20-23] Nevertheless, more recently the interest has been addressed towards bio-medical applications, ranging from tissue engineering to platforms for cell culture investigations.[24-27] The control of the cell–substrate biophysical interactions, through the 3D microenvironment and the surface topography, allows addressing cell adhesion, shape, migration, proliferation and differentiation. In this regard, the clear advantage offered by photosensitive materials relies on the ability to modulate dynamically the relationship between cells and substrate topography.

Since the first works in the nineties,[28, 29] optically induced mass transport in azopolymer films has been implemented to generate reconfigurable topographical patterns (surface relief gratings,

SRGs), with depth in the 1-100μm range depending on the light (intensity, phase and polarization) configuration of interfering beams.[30-32] The starting driving mechanism is the light induced multiple photoisomerization transitions that cause a local orientation of the azobenzene groups axis perpendicular with respect to the E-field vector. When the light has spatial variations of the intensity or of the polarization, local anisotropies within the polymer film (liable to local variations of polarization, free volume, density, molecular ordering of the azo-groups) are induced. This basic phenomenology has been used to develop a series of theoretical models able to support experimental findings,[9, 33-38] however the complete understanding of the processes involved in the surface deformation is still discussed by the scientific community.[39-43]

In gradients of light intensity, generally, the irradiated matter moves towards dark region, and the irradiation with interference patterns of parallel polarized beams gives rise to SRG where the surface relief minima correspond to the light intensity maxima. Several mechanisms have been proposed to explain the origin of the driving force responsible for SRG, including thermal gradients, pressure gradients, permittivity gradients, electric force gradients resulting from the photoinduced anisotropy of the material. However, the involved processes appear to be more complex when light polarization patterns are involved and the proposed models are unsuccessful to fully account for the recorded surface structures. One of the puzzling problems is for example a model able to give a complete explanation of the SRGs induced by different polarization patterns. Electromagnetic force on "photoplasticized" amorphous azopolymer films,[37] as well the recently developed theory of photo-isomerization induced vectorial motion of matter[38] fail in predicting the formation of SRG for linearly polarized s-p configuration of the interfering beams, where the creation of SRG with a periodicity twice that of the light pattern is created.

In this paper, we report on the surface patterning of an amorphous poly-methacrylate[44] film under irradiation with selected 1D polarization interference patterns (PIP), and propose a formulation of the Lorentz driving force density,[37] which includes the both linear and circular photoanisotropies in the complex electric susceptibility tensor[45] induced by the photoisomerization of the azobenzene moieties. The most influential theory by Yang et al. is based on the electromagnetic Lorentz force density but, assuming homogeneous and isotropic electric susceptibility, fails in accounting for the existence of SRGs for the SP configurations.[37] The spatial modulation of the permittivity in the formation of SRGs was considered by Baldus et al. [46] and Inoue et al. [47] to extend the early "gradient force" model.[34] However, the above formulations are limited to the sole Coulomb term of the Lorentz force density, and have been only applied to intensity interference patterns (IIP) generated by parallel linearly polarized beams, also in the presence of an assisting beam, spatially uniform and with orthogonal polarization. Beside the interference of two opposite, right- and left-, circularly (OC) polarized beams, also the superposition of two orthogonal linearly (OL) polarized beams, with different azimuthal angle with respect to the grating wavevector, have been investigated in order to correlate the SRGs features with the PIPs, exploring the range between the usual SP and ±45° configurations. The experimental results are discussed and explained in term of the driving force density model proposed here, which well accounts for the existence, spatial periodicity, relative depth and even the shape of the SRGs obtained by PIPs, including the SP configuration.

Experimental Section

The azopolymer used for the present investigation is a polymethacrylate characterized by a dimeric repeating unit containing both 4-cyanoazobenzene and 4-cyanobiphenyl calamitic moieties employing ester linking groups (in Figure 1, P-eCNB/AZO).[44] The photoresponsive polymer has been properly structured in order to give a high response to the light stimulation in term of photoinduced optical anisotropies and related optomechanical processes inducing surface structuring.[17, 45, 48]

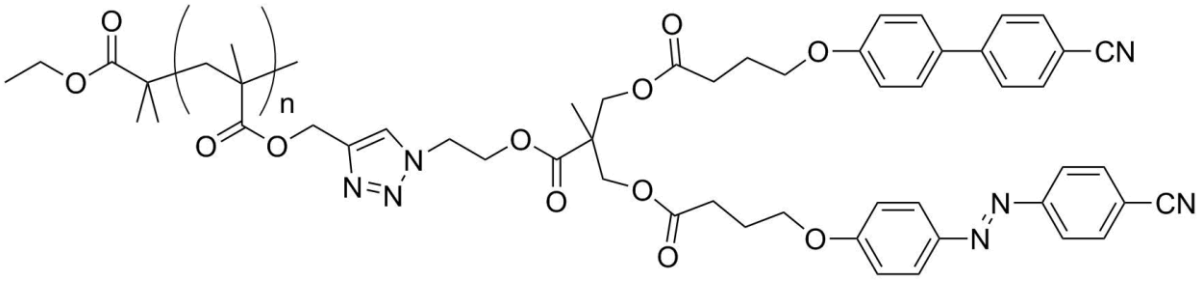

Figure 1. Structure of the polymer P-eCNB/AZO.

The sample is prepared by melting the polymer at T = 120°C, well above the T_g, between two glass plates. After cooling it down to room temperature, one of the confining plates is removed, obtaining a 6.4 μm thick film on top of a glass substrate, with a flat polymer-air interface. The polymer film is then exposed to the PIPs obtained by the interference of two, equally intense, coherent Gaussian beams (λ_{pump} = 457.9 nm, Ar^+ laser Innova 90C, Coherent Inc.), with orthogonal polarizations. The two beams propagate close to the z-axis (see Figure 2a) and cross at a small angle $2\alpha \cong 1.3°$, yielding an optical periodicity $\Lambda = \lambda/2 \sin \alpha \cong 20\mu m$. Given the small crossing angle between the recording beams, intensity modulation is negligible, and the total field polarization ellipse is approximately confined in the xy-plane for all the orthogonal polarization configurations, allowing the use of the Jones-vector formalism.

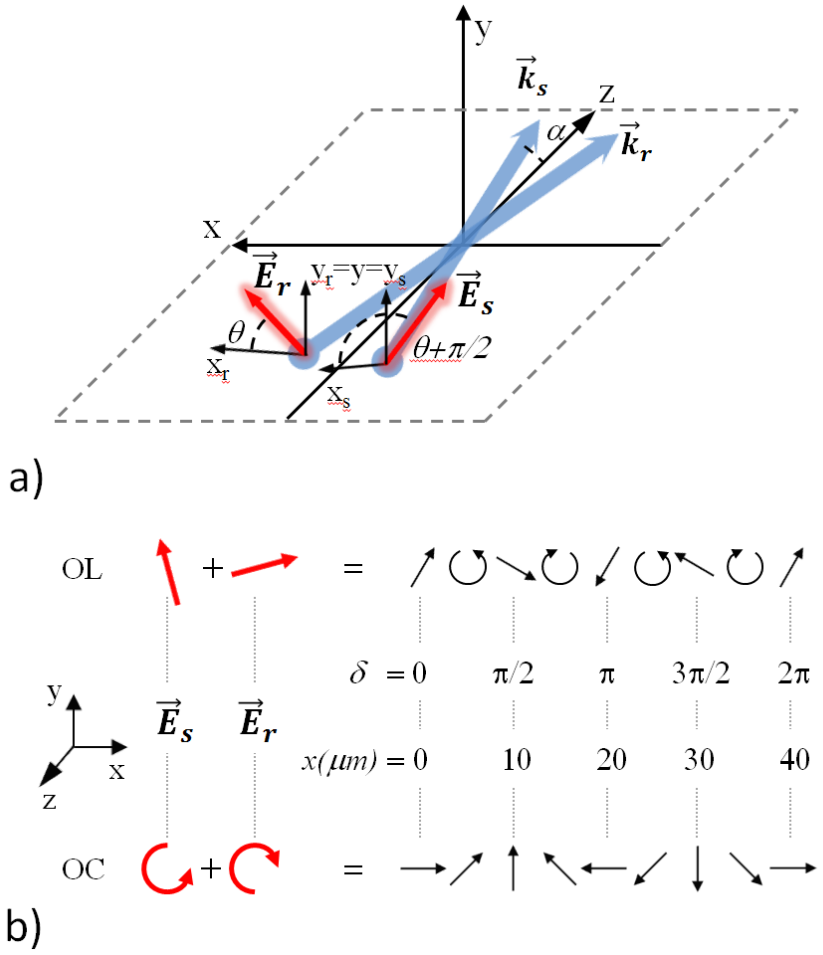

Figure 2. (a) Schematic diagram of the recording geometry in the laboratory xyz frame. The wavevectors $\vec{k}_r$ and $\vec{k}_s$ of the interfering beams lie in the xz plane and make an angle α with the z axis. The xy plane is the free surface of the polymer sample. The electric field of the "reference" $\vec{E}_r$ ("signal" $\vec{E}_s$) beam is sketched in the orthogonal linear (OL) polarization configuration, oriented at an angle θ ($90°+\theta$) with respect to the x_r (x_s) axis. (b) Polarization patterns generated by the interference of orthogonal linearly (OL) and circularly (OC) polarized plane waves. The polarization patterns are sketched versus the x coordinate and the half phase difference between the recording waves $\delta = \pi x/\Lambda$.

In the case of the generalized OL configuration, the electric field of the "reference" (*r*) and the "signal" (*s*) beam forms an angle θ and $90°+\theta$ with the x-axes, respectively (see fig. 2a). The interference field

$$\vec{E}_{OL}(\theta) = \vec{E}_r + \vec{E}_s = \begin{bmatrix}\cos\theta \\ \sin\theta\end{bmatrix} e^{i\delta} + \begin{bmatrix}-\sin\theta \\ \cos\theta\end{bmatrix} e^{-i\delta} = \begin{bmatrix}\cos\delta\,(\cos\theta - \sin\theta) + i\sin\delta\,(\cos\theta + \sin\theta) \\ \cos\delta\,(\cos\theta + \sin\theta) - i\sin\delta\,(\cos\theta - \sin\theta)\end{bmatrix} \quad (1)$$

where $\delta \equiv \pi x/\Lambda$ is half of the phase difference between the two beams, is depicted in Fig. 2b as a polarization ellipse of constant azimuth ($\pm 45° + \theta$) and spatially modulated ellipticity. Similarly, the interference field of the OC configuration where the *r* and *s* beams are left- and right- circularly polarized, respectively

$$\vec{E}_{OC} = \vec{E}_r + \vec{E}_s = \frac{1}{\sqrt{2}}\begin{bmatrix}1 \\ -i\end{bmatrix} e^{i\delta} + \frac{1}{\sqrt{2}}\begin{bmatrix}1 \\ i\end{bmatrix} e^{-i\delta} = \sqrt{2}\begin{bmatrix}\cos\delta \\ \sin\delta\end{bmatrix} \quad (2)$$

is represented in fig. 2b as a linearly polarized field whose azimuth varies continuously with δ.

The SRGs are recorded by exposing the sample to the PIPs of eqs. 1 and 2, having a total intensity of 200 mW/cm^2 for writing time of 12 minutes. The OL SRGs are recorded at four different values of θ, namely 0, 15°, 30° and 45°. The topography of the SRGs is investigated by a profilometer (Dektak 8, Veeco) and an atomic force microscope (AFM, MultiMode 8, Bruker) operated in tapping mode, right after the recording process, *ex-situ*, therefore the spatial phase between the SRGs and the polarization pattern cannot be evaluated from the experiment.

Results and Discussion

In Figures 3 the AFM surface topographies (on the right) and the height profiles (on the left) of the SRGs recorded by the PIPs of eqs.1 and 2 (Figure 2b), are reported. Figure 3a refers to the SRG obtained by illumination with the OC configuration, which is among the most efficient PIPs.[49]

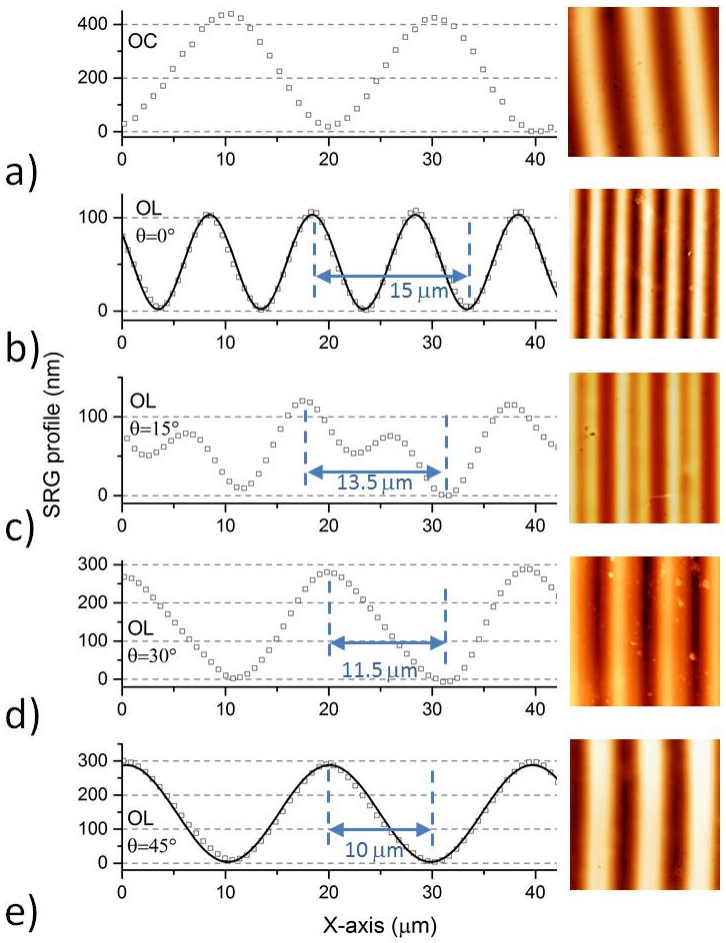

Figure 3. Height profiles (open squares) of the SRGs recorded with (a) OC configuration and OL configuration with (b) θ=0°, (c) θ=15°, (d) θ=30° and (e) θ=45°. Solid black lines in (b) and (e) are sinusoidal fits of the measured profiles. On the right, AFM imaging of the surface topography is reported for the different SRGs.

The topography, characterized by a sinusoidal profile, has a depth of about 400nm and the same spatial periodicity Λ = 20 µm of the polarization pattern. Interesting results are found by investigating the topography of the polymer films after irradiation with the OL PIPs, with different angle $0° \leq \theta \leq 45°$ (Fig. 3b-e). The OL PIPs at θ = 0°, which corresponds to the usual SP configuration, also creates a sinusoidal profile, with the expected periodicity equal to $\Lambda/2$, in

agreement with the results reported in the literature,[50,51] and a substantial depth of about 100nm (Fig. 3b). The rotation of the linear polarizations of the interfering beams by θ in the range (0°-45°] breaks the symmetry of the SP PIP and causes the spatial periodicity of the SRGs to switch from $\Lambda/2$ to Λ (Fig. 3c-e). The transition in the reliefs shape between the sinusoidal profiles observed at $\theta = 0°$ and $\theta = 45°$ is depicted in Fig. 3c-d. Comparing the curves for $\theta = 0°$ (Fig. 3b) and $\theta = 15°$ (Fig. 3c), it is evident that consecutive peaks of the former profile are enhanced and suppressed, respectively, in the latter profile, while the distances between extremants (global/local minima and maxima) are reduced. In particular, the distance between a peak and the second next valley diminishes from 15 μm at $\theta = 0°$ (Fig. 3b), to about 13.5, 11.5 and 10 μm at $\theta = 15°$, 30° and 45°, respectively. The overall depth of the reliefs progressively increases and reaches its maximum value of 300 nm for $\theta = 45°$.

In order to rationalize the experimental outcomes described above and to elucidate the dependence of the SRGs amplitude, periodicity and shape on the OL PIPs, we generalize the model based on the Lorentz force inside the material proposed by Yang et al. .[37] We drop the assumption of homogeneous and isotropic medium and include the spatial modulation of the electric susceptibility tensor, which accounts for the photo-induced linear and circular optical anisotropies, typical of azobenzene polymers.

The electromagnetic force per unit of volume according to the Lorentz formulation is:

$$\vec{f} = -\left(\nabla \cdot \vec{P}\right)\vec{E} + \frac{\partial \vec{P}}{\partial t} \times \vec{B} \qquad (3)$$

where $\vec{E}$ and $\vec{B}$ are the total electric field and magnetic induction, $\vec{P} = \varepsilon_0 \bar{\bar{\chi}} \vec{E}$ is the polarization of the medium, and we have assumed zero free charge and current density and magnetization. The net driving force density responsible of SRGs formation is the time-averaged force:

$$\langle \vec{f} \rangle_t = -\langle \left(\nabla \cdot \vec{P}\right)\vec{E} \rangle_t + \langle \vec{P} \times \left(\nabla \times \vec{E}\right) \rangle_t \qquad (4)$$

Our photoanisotropic material, based on an orientationally dependent photoisomerization responsible of photoinduced dichroism and/or birefringence, can be described by considering a photoanisotropic nonlinear response to parallel and perpendicular polarization ($\hat{k}_{\parallel}$ and $\hat{k}_{\perp}$), as well as a response to the circular polarization $\hat{k}_c$ [44,48] in the more general case.

The complex electric susceptibility tensor $\bar{\bar{\chi}}$ has been written, in the laboratory xyz frame, according to the approach reported in the ref. 45 to calculate $\vec{P}$ in eq. (4). It is a spatially varying 3×3 tensor that relates the changes of the complex susceptibility to the coherency matrix elements ($J_{lm} \equiv E_l E_m^*$ with *l, m* = x, y) of the interference fields:

$$\bar{\bar{\chi}} = \begin{bmatrix} \hat{\chi}_0 + \hat{k}_{\parallel} J_{xx} + \hat{k}_{\perp} J_{yy} & \frac{(\hat{k}_{\parallel} - \hat{k}_{\perp})(J_{xy} + J_{yx})}{2} + \hat{k}_c (J_{xy} - J_{yx}) & 0 \\ \frac{(\hat{k}_{\parallel} - \hat{k}_{\perp})(J_{xy} + J_{yx})}{2} - \hat{k}_c (J_{xy} - J_{yx}) & \hat{\chi}_0 + \hat{k}_{\perp} J_{xx} + \hat{k}_{\parallel} J_{yy} & 0 \\ 0 & 0 & \hat{\chi}_0 + \hat{k}_{\perp} (J_{xx} + J_{yy}) \end{bmatrix} \quad (5)$$

where $\hat{\chi}_0$ is the isotropic and homogeneous complex susceptibility of the medium. The time averaged force density component along the grating wavevector (i.e. x component), which would be the main responsible of the SRGs formation, has been calculated for both OC and OL-θ configurations of the interfering fields (eqs. 1 and 2) from eqs. 4 and 5:

$$\langle f_x \rangle_t = -\varepsilon_0 (\hat{\chi}_{xx} \frac{\partial E_x}{\partial x} + \hat{\chi}_{xy} \frac{\partial E_y}{\partial x} + E_x \frac{\partial \hat{\chi}_{xx}}{\partial x} + E_y \frac{\partial \hat{\chi}_{xy}}{\partial x}) E_x^* + \varepsilon_0 (\hat{\chi}_{xy} E_x + \hat{\chi}_{yy} E_y) \frac{\partial E_y^*}{\partial x} \quad (6)$$

in which we have neglected the y and z dependences of E_i and $\hat{\chi}_{ij}$ (*i, j* = x, y, z) because of the uniform irradiation in the y direction. Note that eq. 6 includes both the optically induced gradient force, related to the field amplitudes modulation, and the susceptibility gradient force, due to the photoanisotropy induced by irradiation with modulated polarization.

For the OC configuration the coherency matrix is

$$J_{OC} = \begin{bmatrix} 2\cos^2 \delta & \sin 2\delta \\ \sin 2\delta & 2\sin^2 \delta \end{bmatrix} \quad (7)$$

and the x component of the driving force density is:

$$\langle f_x \rangle_{t,OC} = \varepsilon_0 \frac{\pi}{\Lambda} \{ Re[\hat{\chi}_0 + 2\hat{k}_{\parallel}] 2 \sin 2\delta \} \quad (8)$$

According to eq. 8, the force density exhibits sinusoidal spatial dependence, with periodicity Λ, and the main contribution to its amplitude is related to the real part of the intrinsic susceptibility $\hat{\chi}_0$, much larger than the $\hat{k}_{\parallel}$ one. The x-component of the force density, scaled by $\varepsilon_0 \pi/\Lambda$, is reported as dashed line in Figure 4, together with the related OC polarization pattern.

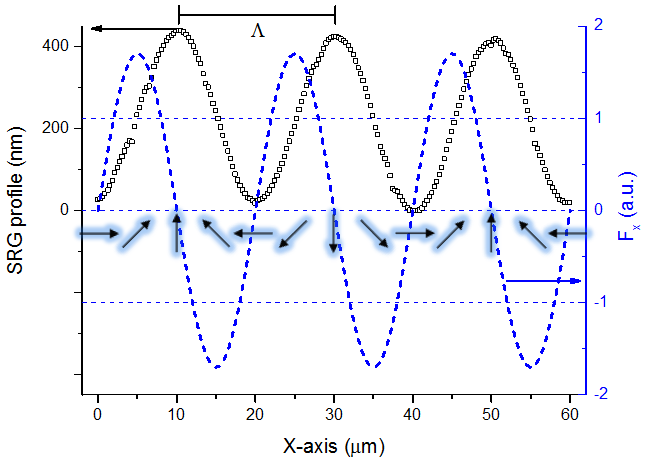

Figure 4. Optical force density profile (dashed blue line) and the corresponding OC polarization pattern are represented along the grating wave vector. The spatial phase of the superimposed SRG profile (black open squares) has been chosen according to the force density.

The spatial phase is such that the force points towards the positive (negative) x direction for $n\pi < \delta < n\pi + \pi/2$ $(n\pi + \pi/2 < \delta < (n+1)\pi)$ for n integer. Consequently, it pushes the material out of the regions with horizontal polarization (i.e. parallel to the grating wavevector) towards the regions with vertical polarization, under the homogeneous softening of the materials induced by the uniform irradiation. Guided by the force density profile, we can now define the absolute spatial phase of the topographic profile (solid line in Fig. 4) with respect to the OC PIP, by assigning the valleys and peaks to the horizontal and vertical polarization position, respectively.

Such correspondence between the SRG and the PIP is in agreement with some experimental investigations based on the diffraction efficiency method,[52] nevertheless it disagrees with the *in-situ* AFM investigation performed by Yadavalli et al. .[53]

For the OL configurations the coherency matrix is:

$$J_{OL}(\theta) = \begin{bmatrix} 1 - \sin 2\theta \cos 2\delta & \cos 2\theta \cos 2\delta + i \sin 2\delta \\ \cos 2\theta \cos 2\delta - i \sin 2\delta & 1 + \sin 2\theta \cos 2\delta \end{bmatrix} \quad (9)$$

and the x component of the driving force density is:

$$\langle f_x \rangle_{t,OL} = \varepsilon_0 \frac{\pi}{\Lambda} \{ -Re\left[\hat{\chi}_0 + 2\hat{k}_{\parallel}\right] 2 \sin 2\delta \sin 2\theta + Re\left[\hat{k}_{\parallel} - \hat{k}_{\perp} - 2\hat{k}_c\right] \sin 4\delta - Im\left[\hat{k}_{\parallel} - \hat{k}_{\perp} - 2\hat{k}_c\right] 2 \cos 4\delta \cos 2\theta \} \quad (10)$$

The first component of the driving force density is similar to the one obtained for the OC configuration, except for the sign and the $\sin 2\theta$ coefficient, that reduces its weight when the angle θ approaches zero. The second and third terms have periodicity $\Lambda/2$, opposite phase and amplitudes related to the real and imaginary part of the same effective photoresponse coefficient $\hat{k}_{eff} \equiv \hat{k}_{\parallel} - \hat{k}_{\perp} - 2\hat{k}_c$. The last term reduces to zero when θ approaches 45°. In order to emphasize the role of the material anisotropy in the electromagnetic force we plots the averaged force density of eq. 10, scaled by $\varepsilon_0 \pi/\Lambda$, in the three following cases, i) $Re\left[\hat{k}_{eff}\right] = Im\left[\hat{k}_{eff}\right] = 0$, ii) $Re\left[\hat{k}_{eff}\right] \neq 0, Im\left[\hat{k}_{eff}\right] = 0$ and iii) $Re\left[\hat{k}_{eff}\right] \neq 0, Im\left[\hat{k}_{eff}\right] \neq 0$, for the polarization patterns corresponding to θ = 0°, 15°, 45° (figure 5a). In the case i), neglecting the material photoinduced anisotropies, the force density would depend only on the first term of eq. 10. Therefore, it would vanish identically for the θ = 0° (i.e., SP) configuration, while it would vary sinusoidally along x, with increasing amplitude as θ increases from 0° to 45° (figure 5b). These force profiles fail in explaining both the occurrence of SRGs in the θ = 0° (i.e., SP) configuration and the non-sinusoidal shape of the SRGs observed for 0° < θ < 45°.

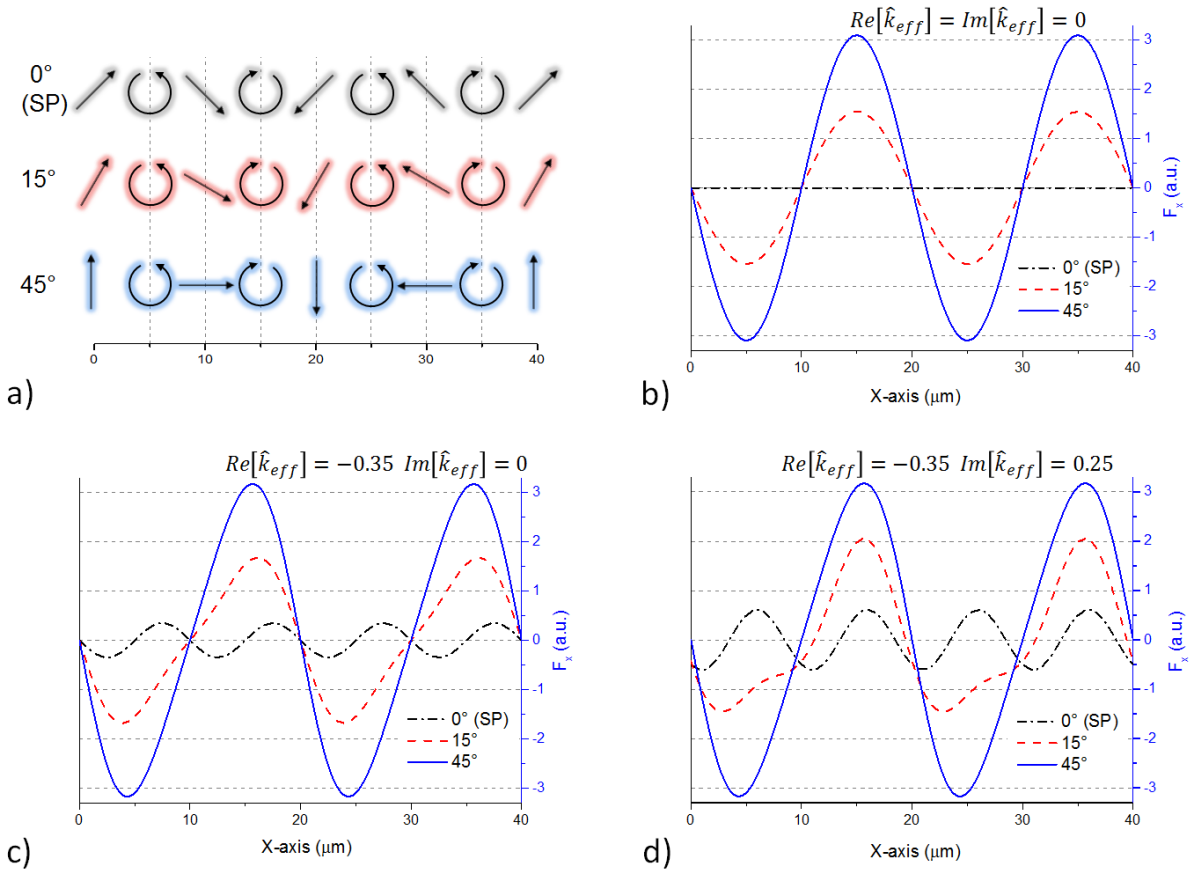

Figure 5. (a) Polarization pattern profiles for OL configuration at different θ values. Optical force density profiles evaluated for (b) $Re[\hat{k}_{eff}] = Im[\hat{k}_{eff}] = 0$, (c) $Re[\hat{k}_{eff}] \neq 0, Im[\hat{k}_{eff}] = 0$ and (d) $Re[\hat{k}_{eff}] \neq 0, Im[\hat{k}_{eff}] \neq 0$.

By assuming $Re[\hat{k}_{eff}] \neq 0$ and $Im[\hat{k}_{eff}] = 0$, the second term in eq. 10 already makes the force density non vanishing for $\theta = 0°$ (figure 5c) and, with a $\Lambda/2 = 10$ μm spatial periodicity, it matches the corresponding SRGs one (figure 3b). We have assumed a negative value for $Re[\hat{k}_{eff}]$ in agreement with the photoinduced orientation of the azobenzenes perpendicular to the light field polarization, which causes a reduction (increase) of the susceptibility in the direction parallel (perpendicular) to the light field polarization (i.e., $Re[\hat{k}_{\parallel}] < 0$ and/or $Re[\hat{k}_{\perp}] > 0$). Moreover, with $Re[\hat{k}_{eff}] < 0$ the phase of the driving force for $\theta = 0°$ (fig. 5c) is compatible with the

experimental observations reported by Yadavalli et al. [50] according to which the maxima of the SRG coincide with the positions of the linear polarizations in the pattern (i.e. x = 0, 10, 20, …μm) (fig. 5a). Nevertheless, by rotating the PIP by $\theta = 15°$ the force profile changes in such a way that former peaks at x = 10, 30, … μm switch to valleys, so that distances between peaks and adjacent valleys are the same. Such prediction is not confirmed by the measurements reported in figure 3c, where it is evident that the distances between a peak and the leading and trailing global minima are different.

By assuming $Re[\hat{k}_{eff}] \neq 0$ and $Im[\hat{k}_{eff}] \neq 0$, (figure 5d), the force function becomes strongly asymmetric displaying unevenly spaced zeros, which is in agreement with the maxima of the measured SRG not centered with respect to the adjacent minima.

In figure 6 the measured SRG have been reported superimposed to the driving force profile and the polarization pattern, positioning the minima of the SRG where the corresponding $f_x(x)$ exhibits zero value and positive derivative. Consequently, the position of the maxima matches the points where the force vanishes with negative derivative, strengthening the suitability of the model with respect to the SRG formation. It is worth noting that the amplitude of the force modulation scales well with the depth of the SRG, this behavior is quantitatively consistent especially for the polarization configurations which provide a sinusoidal profile of the force, i.e for $\theta = 0°$ and 45°. Further developments of the model have to be carried out in order correlate the actual topography with the calculated electromagnetic driving force, taking in to account the mechanical behavior of the material.

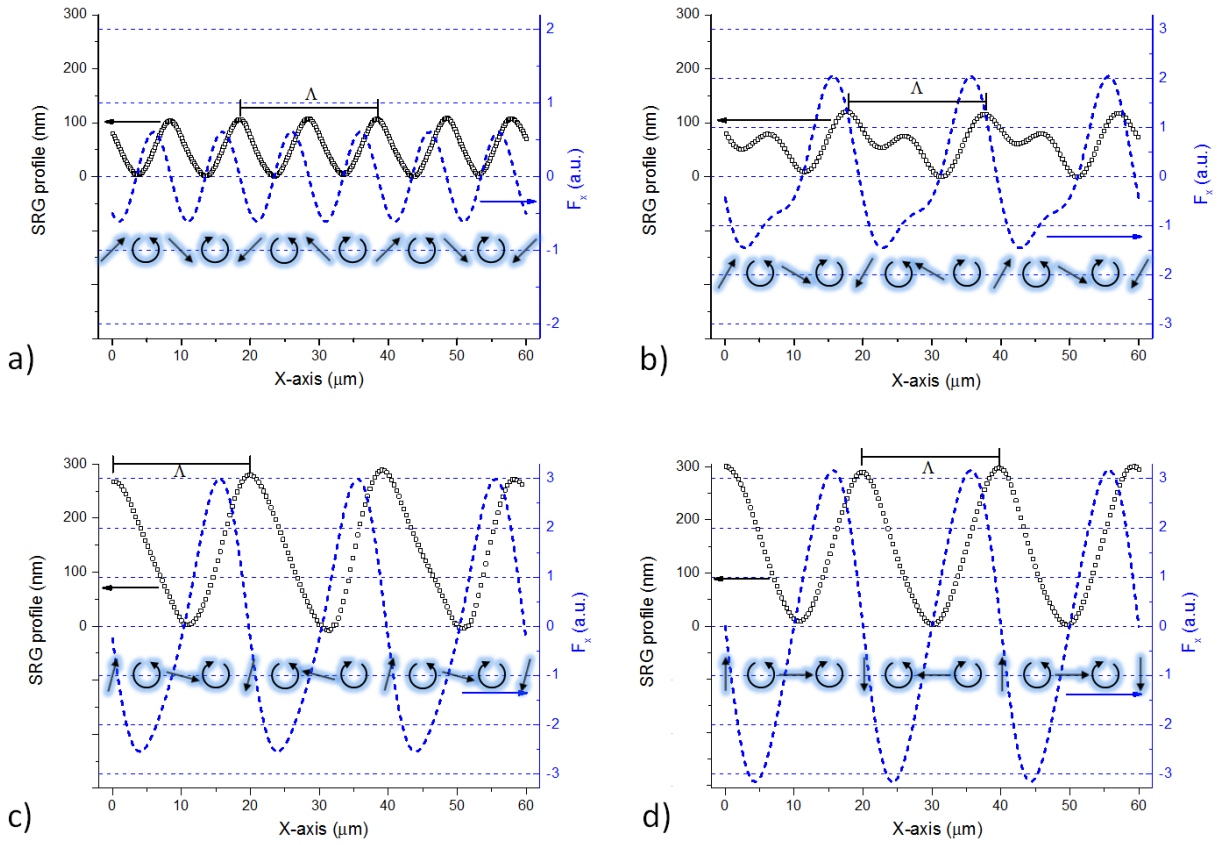

Figure 6. Optical force density profiles (dashed blue lines) and the corresponding OL polarization patterns at (a) θ=0°, (b) θ=15°, (c) θ=30°, (d) θ=45° are represented along the grating wave vector. The spatial phases of the superimposed SRG profiles (black open squares) have been chosen according to the force densities.

In conclusion, we report an experimental study and a generalized force model for the SRGs formation by vectorial holography on an azopolymer film. In the OL polarization case, by changing the angle of the linear polarization with respect to the grating wave vector, from 0° to 45°, we observe how the relief shape changes between the two widely studies configurations, namely SP and ±45°. Both the occurrence of surface relief grating with sinusoidal shape and half periodicity for SP configuration and the asymmetric shape for $0° < \theta < 45°$ have been accounted for by extending the theoretical model of the gradient electric force [37] including the linear and

circular photoanisotropic response of the material in the bulk. The proposed theoretical framework well explains the observed phenomenology associated to the SRGs formation with pure polarization patterns.

AUTHOR INFORMATION

Corresponding Author

*E.mail address: pasquale.pagliusi@fis.unical.it

ORCID

Pasquale Pagliusi: 0000-0001-8077-816X

Author Contributions

P. P. and G. C. conceived the idea, provided regular guidance to the research, and wrote the manuscript. M. P. and L. O. synthesized the polymer. B. A., C. P. and P. P. carried out the experiments. P. P. develops the theoretical model for the driving force and prepared the figures. All the authors discussed the results and commented on the manuscript. All authors have given approval to the final version of the manuscript.

Notes

The authors declare no competing financial interest.

ACKNOWLEDGMENT

The authors thank M. P. De Santo for the AFM imaging of the SRGs topography.

REFERENCES

1. Li, Q., *Intelligent stimuli-responsive materials: from well-defined nanostructures to applications*. John Wiley & Sons: 2013.

2. Aguilar, M. R.; San Román, J., Introduction to smart polymers and their applications. In *Smart polymers and their applications*, Elsevier: 2019; pp 1-11.

3. Wei, M.; Gao, Y.; Li, X.; Serpe, M. J., Stimuli-responsive polymers and their applications. *Polymer Chemistry* **2017**, *8*, 127-143.

4. Zhang, J., *Switchable and responsive surfaces and materials for biomedical applications*. Elsevier: 2014.

5. Zhao, Y.; Ikeda, T., *Smart light-responsive materials: azobenzene-containing polymers and liquid crystals*. John Wiley & Sons: 2009.

6. Vapaavuori, J.; Bazuin, C. G.; Priimagi, A., Supramolecular design principles for efficient photoresponsive polymer–azobenzene complexes. *Journal of Materials Chemistry C* **2018**, *6*, 2168-2188.

7. Weigert, F., Photodichroismus und Photoanisotropie. I. *Zeitschrift für Physikalische Chemie* **1929**, *3*, 377-388.

8. Nikolova, L.; Todorov, T.; Ivanov, M.; Andruzzi, F.; Hvilsted, S.; Ramanujam, P., Photoinduced circular anisotropy in side-chain azobenzene polyesters. *Optical Materials* **1997**, *8*, 255-258.

9. Viswanathan, N. K.; Balasubramanian, S.; Li, L.; Tripathy, S. K.; Kumar, J., A detailed investigation of the polarization-dependent surface-relief-grating formation process on azo polymer films. *Japanese Journal of Applied Physics* **1999**, *38*, 5928-5937.

10. Natansohn, A.; Rochon, P., Photoinduced motions in azo-containing polymers. *Chemical Reviews* **2002**, *102*, 4139-4176.

11. Viswanathan, N.; Kim, D.; Tripathy, S., Surface relief structures on azo polymer films. *Journal of Materials Chemistry* **1999**, *9*, 1941-1955.

12. Shibaev, V.; Bobrovsky, A.; Boiko, N., Photoactive liquid crystalline polymer systems with light-controllable structure and optical properties. *Progress in Polymer Science* **2003**, *28*, 729-836.

13. Tejedor, R. M.; Millaruelo, M.; Oriol, L.; Serrano, J. L.; Alcalá, R.; Rodríguez, F. J.; Villacampa, B., Photoinduced supramolecular chirality in side-chain liquid crystalline azopolymers. *Journal of Materials Chemistry* **2006**, *16*, 1674-1680.

14. Zhao, Y.; He, J., Azobenzene-containing block copolymers: the interplay of light and morphology enables new functions. *Soft Matter* **2009**, *5*, 2686-2693.

15. Hendrikx, M.; Schenning, A.; Debije, M.; Broer, D., Light-triggered formation of surface topographies in azo polymers. *Crystals* **2017**, *7*, 231.

16. Karageorgiev, P.; Neher, D.; Schulz, B.; Stiller, B.; Pietsch, U.; Giersig, M.; Brehmer, L., From anisotropic photo-fluidity towards nanomanipulation in the optical near-field. *Nature materials* **2005**, *4*, 699-703.

17. Provenzano, C.; Pagliusi, P.; Cipparrone, G.; Royes, J.; Piñol, M.; Oriol, L., Polarization holograms in a bifunctional amorphous polymer exhibiting equal values of photoinduced linear and circular birefringences. *The Journal of Physical Chemistry B* **2014**, *118*, 11849-11854.

18. Nikolova, L.; Ramanujam, P. S., *Polarization holography*. Cambridge University Press: 2009.

19. Nikolova, L.; Todorov, T.; Ivanov, M. T.; Andruzzi, F.; Hvilsted, S.; Ramanujam, P., Polarization holographic gratings in side-chain azobenzene polyesters with linear and circular photoanisotropy. *Applied Optics* **1996**, *35*, 3835-3840.

20. Brown, D.; Natansohn, A.; Rochon, P., Azo polymers for reversible optical storage. 5. Orientation and dipolar interactions of azobenzene side groups in copolymers and blends containing methyl methacrylate structural units. *Macromolecules* **1995**, *28*, 6116-6123.

21. Rasmussen, P. H.; Ramanujam, P.; Hvilsted, S.; Berg, R. H., A remarkably efficient azobenzene peptide for holographic information storage. *Journal of the American Chemical Society* **1999**, *121*, 4738-4743.

22. Shishido, A., Rewritable holograms based on azobenzene-containing liquid-crystalline polymers. *Polymer Journal* **2010**, *42*, 525-533.

23. Yager, K. G.; Barrett, C. J., Azobenzene polymers for photonic applications. *Smart light-responsive materials* **2009**, *1*, 1-46.

24. Rocha, L.; Păiuş, C.-M.; Luca-Raicu, A.; Resmerita, E.; Rusu, A.; Moleavin, I.-A.; Hamel, M.; Branza-Nichita, N.; Hurduc, N., Azobenzene based polymers as photoactive supports and

micellar structures for applications in biology. *Journal of Photochemistry and Photobiology A: Chemistry* **2014**, *291*, 16-25.

25. Rosales, A. M.; Mabry, K. M.; Nehls, E. M.; Anseth, K. S., Photoresponsive elastic properties of azobenzene-containing poly (ethylene-glycol)-based hydrogels. *Biomacromolecules* **2015**, *16*, 798-806.

26. Ruskowitz, E. R.; DeForest, C. A., Photoresponsive biomaterials for targeted drug delivery and 4D cell culture. *Nature Reviews Materials* **2018**, *3*, 17087.

27. Fedele, C.; Netti, P.; Cavalli, S., Azobenzene-based polymers: emerging applications as cell culture platforms. *Biomaterials science* **2018**, *6*, 990-995.

28. Rochon, P.; Batalla, E.; Natansohn, A., Optically induced surface gratings on azoaromatic polymer films. *Applied Physics Letters* **1995**, *66*, 136-138.

29. Kim, D.; Tripathy, S.; Li, L.; Kumar, J., Laser-induced holographic surface relief gratings on nonlinear optical polymer films. *Applied Physics Letters* **1995**, *66*, 1166-1168.

30. Priimagi, A.; Shevchenko, A., Azopolymer-based micro-and nanopatterning for photonic applications. *Journal of Polymer Science Part B: Polymer Physics* **2014**, *52*, 163-182.

31. Hsu, C.; Xu, Z.; Wang, X., Holographic Recording and Hierarchical Surface Patterning on Periodic Submicrometer Pillar Arrays of Azo Molecular Glass via Polarized Light Irradiation. *Advanced Functional Materials* **2018**, *28*, 1802506.

32. Bagheri, S.; Giessen, H.; Neubrech, F., Large-Area Antenna-Assisted SEIRA Substrates by Laser Interference Lithography. *Advanced Optical Materials* **2014**, *2*, 1050-1056.

33. Yager, K. G.; Barrett, C. J., All-optical patterning of azo polymer films. *Current opinion in solid state and materials science* **2001**, *5*, 487-494.

34. Kumar, J.; Li, L.; Jiang, X. L.; Kim, D.-Y.; Lee, T. S.; Tripathy, S., Gradient force: The mechanism for surface relief grating formation in azobenzene functionalized polymers. *Applied Physics Letters* **1998**, *72*, 2096-2098.

35. Lefin, P.; Fiorini, C.; Nunzi, J.-M., Anisotropy of the photo-induced translation diffusion of azobenzene dyes in polymer matrices. *Pure and Applied Optics: Journal of the European Optical Society Part A* **1998**, *7*, 71-82.

36. Baldus, O.; Zilker, S., Surface relief gratings in photoaddressable polymers generated by cw holography. *Applied Physics B* **2001**, *72*, 425-427.

37. Yang, K.; Yang, S.; Kumar, J., Formation mechanism of surface relief structures on amorphous azopolymer films. *Physical Review B* **2006**, *73*, 165204.

38. Sekkat, Z., Vectorial motion of matter induced by light fueled molecular machines. *OSA Continuum* **2018**, *1*, 668-681.

39. Saphiannikova, M.; Toshchevikov, V.; Ilnytskyi, J., Photoinduced deformations in azobenzene polymer films. *Nonlinear Opt., Quantum Opt* **2010**, *41*, 27-57.

40. Juan, M. L.; Plain, J. R. M.; Bachelot, R.; Royer, P.; Gray, S. K.; Wiederrecht, G. P., Multiscale model for photoinduced molecular motion in azo polymers. *ACS nano* **2009**, *3*, 1573-1579.

41. Ciobotarescu, S.; Hurduc, N.; Teboul, V., How does the motion of the surrounding molecules depend on the shape of a folding molecular motor? *Physical Chemistry Chemical Physics* **2016**, *18*, 14654-14661.

42. Ambrosio, A.; Marrucci, L.; Borbone, F.; Roviello, A.; Maddalena, P., Light-induced spiral mass transport in azo-polymer films under vortex-beam illumination. *Nature communications* **2012**, *3*, 989.

43. Fabbri, F.; Lassailly, Y.; Monaco, S.; Lahlil, K.; Boilot, J.; Peretti, J., Kinetics of photoinduced matter transport driven by intensity and polarization in thin films containing azobenzene. *Physical Review B* **2012**, *86*, 115440.

44. Roche, A.; García-Juan, H.; Royes, J.; Oriol, L.; Piñol, M.; Audia, B.; Pagliusi, P.; Provenzano, C.; Cipparrone, G., Tuning the Thermal Properties of Azopolymers Synthesized by Post-Functionalization of Poly (propargyl Methacrylate) with Azobenzene Azides: Influence on the Generation of Linear and Circular Birefringences. *Macromolecular Chemistry and Physics* **2018**, *219*, 1800318.

45. Huang, T.; Wagner, K., Coupled mode analysis of polarization volume hologram. *IEEE journal of quantum electronics* **1995**, *31*, 372-390.

46. Baldus, O.; Zilker, S., Surface relief gratings in photoaddressable polymers generated by cw holography. *Applied Physics B* **2001**, *72*, 425-427.

47. Inoue, N.; Nozue, M.; Yamane, O.; Umegaki, S., Driving force for formation of a surface relief grating on an azobenzene-containing polymer. *Journal of Applied Physics* **2008**, *104*, 023106.

48. Royes, J.; Provenzano, C.; Pagliusi, P.; Tejedor, R. M.; Piñol, M.; Oriol, L., A bifunctional amorphous polymer exhibiting equal linear and circular photoinduced birefringences. *Macromolecular rapid communications* **2014**, *35*, 1890-1895.

49. Audorff, H.; Walker, R.; Kador, L.; Schmidt, H.-W., Polarization dependence of the formation of surface relief gratings in azobenzene-containing molecular glasses. *The Journal of Physical Chemistry B* **2009**, *113*, 3379-3384.

50. Yadavalli, N. S.; Santer, S., In-situ atomic force microscopy study of the mechanism of surface relief grating formation in photosensitive polymer films. *Journal of Applied Physics* **2013**, *113*, 224304.

51. Sobolewska, A.; Miniewicz, A., On the inscription of period and half-period surface relief gratings in azobenzene-functionalized polymers. *The Journal of Physical Chemistry B* **2008**, *112*, 4526-4535.

52. Ramanujam, P.; Nedelchev, L.; Matharu, A., Polarization holographic and surface-relief gratings at 257 nm in an amorphous azobenzene polyester. *Optics letters* **2003**, *28*, 1072-1074.

53. Yadavalli, N. S.; Korolkov, D.; Moulin, J.-F. O.; Krutyeva, M.; Santer, S., Probing opto-mechanical stresses within azobenzene-containing photosensitive polymer films by a thin metal film placed above. *ACS applied materials & interfaces* **2014**, *6*, 11333-11340.

For Table of Contents Only